 doi:10.20944/preprints201901.0261.v1

Article

The Assessment of Different Component Analyses in Determining the Post-Glacial Land Uplift Rate by GRACE Data: A Case Study in Fennoscandia and Laurentia

Mehdi S. Shafiei Joud *, Lars Erik Sjöberg and Mohammad Bagherbandi

Division of Geodesy and Satellite Positioning, Royal Institute of Technology (KTH), SE-10044 Stockholm, Sweden; Faculty of Engineering and Sustainable Development, University of Gävle, SE-80176 Gävle, Sweden, lars.sjoberg@abe.kth.se (L.S.), mohbag@kth.se (M.B.)
Sweden.
* Correspondence: smsj@kth.se

Abstract: The mantle mass flow interconnected with the process of Glacial Isostatic Adjustment (GIA) and the reformation of the Earth's crust constantly perturbs the observed gravity field towards a hypothetic isostatic state. We analyse the temporal changes of the gravity field from the GRACE data, using different mathematical and/or statistical methods to detect the GIA amidst other gravity signals. A number of gravimetric post-glacial land uplift rate (LUR) modelling methods are investigated and compared with the data from a total number of 515 GPS stations and preferred GIA forward models in Fennoscandia and North America. We investigate three mathematical methods, namely regression, principal component, and independent component analysis (ICA) to extract the GIA signal from the GRACE monthly geoid heights. We use some regularization techniques to exploit the GRACE monthly data to their maximum spatial resolution and to increase the Signal to Noise Ratio of their short wavelengths. Near the centres of the study areas the gravimetric LUR model using the fast-ICA algorithm of Hyvärinen and Oja (2000) is shown to be in a complete agreement with the GPS data and the predictions of the GIA forward models, and for the whole epeirogeny regions, their discrepancies reach to the extrema at -1.8 and +3.3, and -4.5 and +7.5 mm/a, respectively. We show that the largest discrepancies between the gravimetric model using the ICA method and the GIA forward model, occur for the sub-regions likely collocated with strong ice mass change signals.

Keywords: Glacial Isostatic Adjustment; gravimetric land uplift rate modelling; GRACE; independent component analysis

1. Introduction

The Glacial Isostatic Adjustment (GIA) process, i.e. the viscos response of the Earth's interior and adjustment of its surface to the removal of the ice loads following several periods of ice ages, relates to a mass transfer under the Earth's crust, therefore causing temporal changes in the observed gravity signal. Gravity also varies while the land deforms during the rebounding process. In certain areas of the Earth's surface, the solid Earth movement due to GIA can be observed, among which we select Fennoscandia and Laurentia. The data of the solid Earth movements in these areas have been attributed a long-time record including tide gauges, paleo-shoreline, precise levelling and GPS data, which provide a rich data set to compare with the gravity data. It was not earlier than in the 1980s that gravity measurements played its important role in GIA studies [1].

Traditionally, gravity changes have been determined by repeated measurements using relative and absolute gravimeters on the terrestrial gravimetric networks established in the rebounding areas, such as the Fennoscandian 63° latitude gravity line. This network was analysed by [2] who estimated

Preprints (www.preprints.org) | NOT PEER-REVIEWED | Posted: 25 January 2019 doi:10.20944/preprints201901.0261.v1

a gravity change /land uplift rate at −0.22 μGal⁄mm and [3] (-0.16±0.04 μGal⁄mm). [4] estimated the secular trend of gravity at -1.52±0.20 and +1.00±0.14 μGal⁄a at the western and the eastern part of the line, respectively. The Nordic Geodetic Commission organized the measurements in Fennoscandia. For GIA studies an accuracy of sub-μGal per annum for the temporal gravity change is needed (see e.g. [5]). The use of gravity measurements for GIA studies did not appear until the 1980s by reestablishment of the gravimetry networks with more accurate apparatus. In the Laurentian area, relative gravity observations have been obtained for about five decades on the Canadian Gravity Standardization Network (CGSN) using primarily LaCoste-Romberg gravimeters that have a sufficient precision as mentioned above [5]. These data are analysed by [6] who estimated the mean secular trend at -1.71±0.23 μGal⁄a for Churchill, Manitoba at the south-eastern coast of the Hudson Bay, [5] who found -2.35±0.06 and -1.71±0.06 μGal⁄a at the south-east and south-west coast of the Hudson Bay and [7] who estimated a slope of -0.18 ± 0.03 μGal⁄mm.

The Gravity Recovery And Climate Experiment (GRACE) twin satellites (2002-2017) mission designed to detect the temporal variations of gravity has proved to be feasible for numerous applications. The applications of GRACE data were mainly addressed in studying the mass transport between the cryosphere, oceans and groundwater reservoirs. Yet, the GRACE observed gravity signal and its global coverage can provide the opportunity to study the mass change inside the Earth. The GRACE gravity change signal is a superposition of the gravity signals of many processes with different temporal and spatial scales, implying that the time series of the GIA signal needs to be extracted amidst the other disturbing gravity signals, such as hydrology.

[8] performed a simulation using five years, the expected life-time of the mission, of synthetic data. They showed that GRACE can provide a secular trend for the Laurentian rebound region, which to a certain harmonic degree is more accurate than the discrepancies among some preferred geophysical GIA models. [9] used the absolute gravity observations of CGSN and GPS vertical velocities from the Canadian Base Network (CBN), which included almost four decades of gravity observations and more than 10 years of GPS measurements. They processed the geoid changes using the technique described by [10], and after a supervised data processing strategy, including replacing the harmonics of degree one, the second zonal and using de-striping only for harmonic degrees over $n = 8$, they extracted a secular trend using the Principal Component Analysis/Empirical Orthogonal Functions (PCA/EOF) method.

[11] generated a combined model for Fennoscandia by assimilating sea level variation data from tide gauges, solid land vertical movement from GPS data and nearly six years of GRACE free-air gravity anomaly rates into a preferred geophysical GIA model, after modelling and removing the water storage from the Global Land Data Assimilation Systems (GLDAS) model. The GRACE data was processed using the technique described by [10], and therefore, sampled to a 2° grid. They found a bias between results produced with and without the GRACE data assimilated, which they removed by introducing to the model a constant which they called "uniform gravity rate across the Fennoscandia region".

[12] estimated the secular gravity rates from GRACE and convert them to uplift rates using the approximation formula of [13]. They estimated the conversion error using preferred GIA forward models at 0.23 and 0.13 mm/a, respectively.

[14] integrated the trend rates obtained from absolute gravity measurements in Fennoscandia, mainly those of the Institut für Erdmessung (IfE), with GRACE data up to harmonic degree and order $n, m = 35$, however they constrained their data-derived model with the data from a geophysical model. [15] utilized five years of GRACE monthly gravity field data, up to harmonic degree $n = 35$ in Fennoscandia to extract the secular trends of the land uplift signal. They employed different data processing (filtering) strategies and concluded that the Gaussian filter (GF) with 400 km smoothing radius were still the best choice, even among their ensemble of non-isotropic filters.

[16] performed a simulation to investigate the potential of two independent component analysis (ICA) methods, i.e., the temporal and spatiotemporal ICA, for extracting a secular trend against periodicities in seven years of the GRACE global gravity data and compared them with the extracted signals using the PCA/EOF method. They found that that both ICA methods show slightly higher correlations with the geophysical GIA signal than when a PCA/EOF were used.

Preprints (www.preprints.org) | NOT PEER-REVIEWED | Posted: 25 January 2019 doi:10.20944/preprints201901.0261.v1

[17] compared their ICE-5G (VM5a) GIA model with the GRACE RL05 derived Equivalent Water Height (EWH) in Fennoscandia and Laurentia. They noted that their GIA model fits the low-pass filtered version of the RL05 GRACE data well, whereas application of the hydrology correction somewhat degrades the fit in the formerly ice-covered region. They speculated that the possible reason for the higher discrepancies, when using RL04 GRACE data [18], was the employed de-striping technique. They concluded that the correlated filtering technique of [10] used by [18], was no longer needed when the RL05 product was used, and instead they suggested using a GF.

The main objective of this study is to propose a methodology to generate a gravimetric model of the post-glacial land uplift rate (LUR) without assuming deglacial history and mantle rheology. A common way to reduce for the GIA signal in many applications is to use a GIA forward model. However, the LUR estimates of these models suffer from large uncertainties in the deglaciation history and mantle rheology (see e.g. [19-20]). The input parameters of the forward models are tuned such that their outputs fit the geodetic data sets, such as GPS. A gravimetric model can provide an alternative data set if it is sufficiently independent from the same assumptions in the forward modelling approaches.

To produce a gravimetric LUR model, we assess the performance of three analysis methods in extracting the gravity signal due to GIA from the GRACE monthly gravity field since 2002. We will generate a gravimetric model of land uplift rate (LUR) due to GIA without any reduction for other (disturbing) effects, such as hydrology or tectonics, to discover how close the extracted signals are to the GIA signal. We use the LUR data from GPS and a GIA forward model as two test data sets to compare with our LUR model. These two data sets are correlated with each other, the former is reduced for the tectonics and free from hydrology, while, the latter is constrained with the geodetic data and predicts LUR, among other predictions. Then we discuss the sub-regions where the discrepancies are significant. To create a LUR model, the gravity/geoid rate signal due to GIA needs to convert to solid Earth vertical movement, which can be compared with the GPS data.

The main motivations to introducing a gravimetric LUR model are to provide an independent data set that can be used in GIA studies and a spatially detailed and precise estimation of the solid Earth vertical movement due to GIA. (A precise LUR model is also of great importance to time-tag national height systems in the study areas.) The main question is whether it is possible to accurately estimate the land uplift rate and the geoid change due to GIA using satellite gravimetry without any a priori assumptions on the elapsed glaciation and the Earth's rheology in the vicinity of the disturbing gravity signals.

We convert the monthly GRACE geoid heights to the solid Earth vertical movement, namely Equivalent Land Uplift (ELU) rates using the mathematical treatment from [21] describe in Sect. 2.1. We extract the GIA signal of the ELU rates using RA, PCA/EOF and ICA and the results are given in Sect. 3. The study areas are introduced in Sect. 3.1, and the data from GPS and a geophysical GIA model, needed to compare with our results are given in Sect. 3.2. In Sect. 3.3, the final land uplift rate models using the GRACE data are depicted and in Sect. 3.4 we discuss their compatibilities versus the GPS data and the data from a geophysical GIA modelling approach, which is followed by the selection of the best gravimetric model. Sect. 4 concludes the paper.

2. Extracting the Land Uplift Rates from GRACE Data

We will generate a number of gravimetric LUR models using the GRACE monthly gravity field from April 2002 until July 2015 provided by the University of Texas at Austin, Center for Space Research (CSR), the German Research Centre for Geosciences (GFZ) and the Centre National d'Etudes Spatiales (CNES), Toulouse.

The GRACE monthly gravity field (level-2 data) is estimated from the GRACE intersatellite (k-band) distance measurements and the satellites orbital data (level-1 and level-1B data [22-23]). Usually, the design matrix of the observation equation, when higher degrees spherical harmonic coefficients (SHCs) are desired, is rank-deficient and an erroneous set of SHCs are published. This

Preprints (www.preprints.org) | NOT PEER-REVIEWED | Posted: 25 January 2019 doi:10.20944/preprints201901.0261.v1

implies that the solution must be regularized or, alternatively, the effect of the errors is now treated as stochastic noise. This noise negatively affects the signal-to-noise ratio (SNR). The effect of the noise is particularly apparent on the higher harmonic degrees of the gravity solutions. The common stripe pattern (see e.g. [10]) in the unconstrained monthly gravity field is an effect of the errors on the estimation of the higher harmonics. This noise is reduced and the signal is retrieved using smoothing filters.

The source of this unwanted error (noise) is not completely known but it is presumed to be related to the in-line orbit configuration of the GRACE satellites. The results of some simulations, using four satellite Cartwheel formation, showed that the errors of the new formation are smaller relative to actual GRACE mission, and that the higher degrees of SHCs can be estimated with an acceptable SNR, indicating that the error are reduced, but not entirely vanished, and they behave such as isotropic stochastic noise (the magnitude of the noise changes only by degrees) on the sphere. Moreover, their results were highly dependent to the errors of the background models [24]. Other sources of errors are the uncertainty in the background models of the tidal and non-tidal atmospheric and oceanic mass variations. We search for a suitable post-processing method to explore the GRACE data to their maximum harmonic degree by implementing a post-processing strategy (filtering) to remove the noise. Comparing with GPS data in a simple Regression Analysis (RA), we select the best data processing method (filtering) among an ensemble of Gaussian and non-isotropic filters.

We also test the data from the Centre National d'Etudes Spatiales (CNES), Toulouse, which is already regularized.

The temporal (monthly) gravity change is then converted to the solid Earth vertical movement or, namely, ELU rate, using the formula described in Sect. 2.1. This formula is based on a simple mantle flow and the theory of isostasy and independent from any assumptions of the deglaciation and the rheology of the mantle (cf. [13,25]).

The GIA signal of the ELU rate is extracted using three analysis methods, namely RA, PCA/EOF and ICA (see Appendix). RA extracts the secular linear trend among the presumed periodicities and noise. Using PCA/EOF, a few uncorrelated projections of the GRACE spatiotemporal data matrix are extracted, while ICA extracts the linear combinations which variate independently from each other.

2.1. The relation between the geoid and land uplift rates

Conventionally, the secular gravity change relates to the solid Earth vertical movement using the formula of [25] (Eq. 34) or its approximated version [13] (Eqs. 4, 8). These formulae need information of the mantle rheology and ice load history. We use another relation from [21] which was developed without such assumptions.

As a consequence of de-loading, a residual portion of the disturbing potential originates from the crustal mass of the deformed upper surface (T_P^{up}), while another part is from the deformation at the base of the crust (T_P^{low}). Assuming that the crustal density ρ_c, and the crust/mantle density contrast $\Delta\rho = \rho_m - \rho_c$ are constants, for the radial integration, and a regional Vening Meinesz isostatic model, we eventually use the first order approximation derived in [21]:

$$\left(\dot{\bar{T}}_P\right)_n = \left(\dot{\bar{T}}_P^{up}\right)_n + \left(\dot{\bar{T}}_P^{low}\right)_n \approx 4\pi G\rho_m R\frac{1}{2n+1}\left(\dot{h}_P\right)_n \quad (1)$$

where $\dot{\bar{T}}_P$ is the change in the disturbing potential at P due to the land uplift rate of $\dot{h}$. The Laplace harmonic of degree n is denoted by $(\,)_n$. The approximation to obtain the disturbing potential on the upper/lower surface can be written as:

$$\left(\dot{T}_P^{up/low}\right)_n = \left(\dot{\bar{T}}_P^{up/low}\right)_n + c^{up/low}O(\varepsilon) \quad (2)$$

Preprints (www.preprints.org) | NOT PEER-REVIEWED | Posted: 25 January 2019 doi:10.20944/preprints201901.0261.v1

where the constant $c^{up/low}$ can be either c^{up} or c^{low} and they relate as $c^{up} = (\rho_c/\Delta\rho)c^{low}$. The order of the approximation $O(\square)$ for the land uplift rate can reach 0.01 mm/a for the maximum degree of $n = 90$.

From Eq. (1), the SHC of the temporal change of the disturbing potential ($A_{nm}^{\dot{T}}$), for each degree n and order m, relates to the SHC of the land uplift rate ($A_{nm}^{\dot{h}}$) by [21]:

$$A_{nm}^{\dot{h}} \square \frac{1}{4\pi G\rho_m R}(2n+1)A_{nm}^{\dot{T}} \tag{3}$$

3. Numerical Study

3.1. The Study Areas

Laurentia, or the North American Craton, is the ancient geological core of the North American continent [26]. Our study area is windowed by $22^o \le \varphi \le 85^o$ latitudes and $-143^o \le \lambda \le -19^o$ west longitudes. The uplifting area is about 16503000 km^2 centred at the eastern coast of Hudson Bay [6]. This area also includes Greenland, however, we exclude it, since reliable observations of land uplift rate for its inland areas are not available [27] (p. 111). In addition, hot-spot activities contaminate the GPS data in the eastern coast.

The Fennoscandian rebound region is dominated by bedrocks of the Baltic Shield, which is a part of the old East European Craton. The uplifting area has a spatial extension in northeast-southwest direction of about 2400 km length covering an area of about 3086000 km^2 [28]. Presently, the north-west coast of the Bothnian Gulf is undergoing an uplift rate of about 1 cm/a. Our study area is limited by $48^o \le \varphi \le 81^o$ latitudes and $2^o \le \lambda \le 34^o$ eastern longitudes.

3.2. Data

The Data of the solid Earth vertical movement: For Fennoscandia, we use the GPS solution of [29]. The GPS velocities were analysed using GAMMIT and GIPSY-OASIS, in parallel, on the data from the continuous GPS stations since August 1996. The minimum duration of the recorded data is 3 years. To remove the land movements due to other processes than GIA, [29] defined a moving reference frame using a 3D velocity field from a GIA forward model, which showed the best fit to the land uplift rate data in the area [30]. Then, the 3D GPS velocity field has been translated and rotated to this moving reference frame.

For North America, we use two sets of GPS data. The first data set consists of 239 continuous GPS measurements since 1993, with a minimum record duration of 3 years, and 123 Canadian Base Network (CBN) stations with data longer than 4 years. This is the same data set used by [31], which were processed using GIPSY-OASIS software [32] and the velocities were calculated using a weighted least squares regression (see [32], Table S1). They, additionally, used 124 stations, far from the area affected by the GIA and seismicity, to estimate the best-fit angular velocity for the plate and remove that from the horizontal processed GPS data and, finally, determine the velocities due to GIA. Also, we received some GPS data in SINEX format from [33] since 2000 as well as a set of global sites used to define the reference frame. The repeated CBN stations were also included [34]. Albeit, the newer version of [34] used a longer data set, and a predefined unified reference frame (ITRF2005), instead of using a regional one. However, the newer data set does not include some of the very important stations for GIA studies around Hudson Bay, since their main objective was to fix the reference frame and determine the tectonic movements [33]. To control the process of our analysis method for these important stations, we use the same time-series as [31] used for their solution, while for other stations, we use the GPS measurements up to 2011/03 (GPS week 1621). Then we process them together relative to ITRF2005 using a least squares adjustment. The final GPS data set consists of 362 stations.

The standard errors in estimating the vertical movement for each station are depicted in Fig. 1. We will use these error estimates in forming the test variable when comparing with the GRACE data.

Preprints (www.preprints.org) | NOT PEER-REVIEWED | Posted: 25 January 2019 doi:10.20944/preprints201901.0261.v1

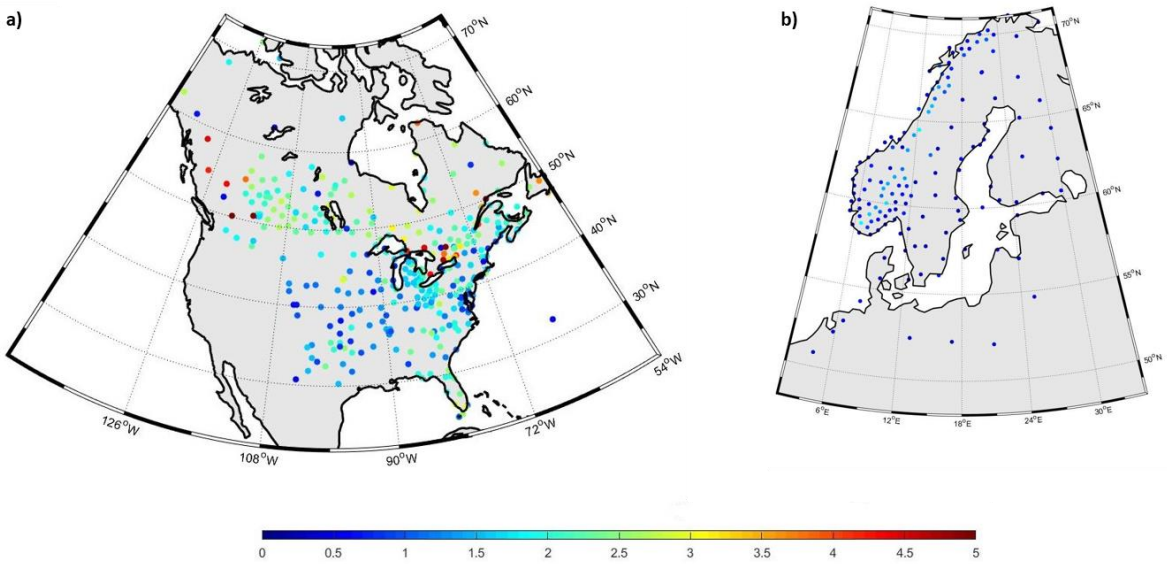

Figure 1. The standard errors of the determination of the GPS land uplift rates for a) North America and b) Fennoscandia [29], at each station.

The GRACE data: We use the fully normalized SHCs of the GRACE monthly solutions of release 5 (RL05a) from CSR [22], GFZ [23] and of the release 3 (RL03) provided by CNES. For this study, 147 GFZ and CSR monthly gravity field solutions from April 2002 until July 2015 are used. The gravitational effect resulting from the atmosphere and oceanic variability are removed using the the Atmospheric and Oceanic De-aliasing product (AOD1B) [35]. AOD1B were reprocessed for the period from October 2013 till July 2014, because the temperature model was not properly fixed and imposed a bias at this time [35]. The data of missing months are linearly interpolated. The maximum degree and order of the spherical harmonics are set to 90 and 96 for the GFZ and CSR data, respectively. The 2nd zonal coefficient of the GFZ monthly data has a reportedly false value, which is replaced by that from the SLR data [23]. In addition, 144 monthly solutions from CNES, complete to degree 80, are used to test an alternative processing technique (http://grgs.obs-mip.fr/grace). There are also other analysis centres with different analysis methods and background models [33,37,23,36].

We use anisotropic filters, namely DDK1 to DDK8 [37] (Table 1, and Eq. 3 for DDK1-3), and isotropic GFs of varying radii (half wavelength at 350-800 km) to smooth the monthly GRACE data (Except the CNES data where a regularization method was already used). The background theory and the relations to generate the GFs were given in [38] (Eq. 53).

The regularization factor of DDKx filters controls the power of the smoothing; from the strongest to the weakest smoothing powers are DDK1, with $\lambda = 1 \times 10^{14}$ to DDK8, with $\lambda = 5 \times 10^{9}$ (high-pass, DDK1, to low-pass, DDK8). For the GFs, the smaller radius means the larger smoothing power. Note that by using smoothing powers larger than $\lambda = 1 \times 10^{14}$ for anisotropic filtering or radii smaller than 350 km, leads to unwanted over smoothing. On the other hand, the anisotropic filters with smoothing powers smaller than $\lambda = 5 \times 10^{9}$ or GFs with radii larger than 750 km, fails to remove the noise.

Preprints (www.preprints.org) | NOT PEER-REVIEWED | Posted: 25 January 2019 doi:10.20944/preprints201901.0261.v1

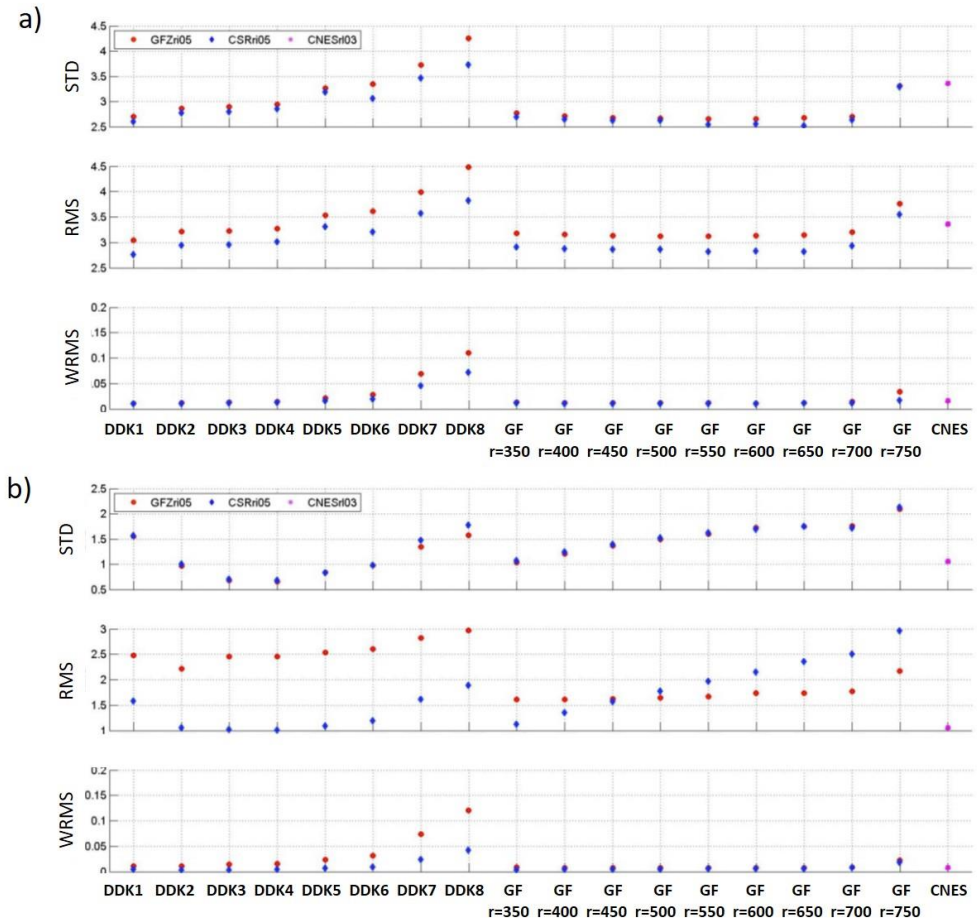

Figure 2. The comparison between the GRACE ELU rate computed using the filters in the abscissa and the regression analysis and the GPS data for a) Laurentia b) Fennoscandia. STD: standard deviation, (W)RMS: (Weighted) Root Mean Squares. Units: mm/a.

To select the best filter, we convolve the weighting functions of the filters with the monthly geoid data, convert them to the ELU rates using Eq. (3), then regress the linear trend and compare with the GPS data at each station. For each study area, the filter which results in the smallest weighted root mean squares ($\mathrm{WRMS} = \frac{1}{N}\sqrt{\sum_{i=1}^{N}\left(\left(\dot{h}_i^{GRACE} - \dot{h}_i^{GPS}\right)s_0 / s_i\right)}$, where s_0 is the estimated standard error of unit weight and N is the number of stations) will be selected to generate the monthly ELU rates.

The selection of the best filter should be carried out after special considerations. The WRMS differences are shown in the last row of Fig. 2. The so-called DDK1~DDK4 and DDK2~DDK4 filters showed the smallest WRMS of the differences for Laurentia and Fennoscandia study areas, respectively. (W)RMS differences of the linear secular trend generated by these filters differ with the GPS data by less than (0.01)0.1 mm/a, which is negligible. Among them, we use DDK4 to smooth our data. DDK4 is associated with a smoothing power of 0.5×10^{11}, which is the smallest one and it reduces the signal damping due to smoothing. We should mention that some of the GFs, which show smaller WRMS are not used in our approach, because they can retrieve the spherical harmonics up to degree 40-50, depending on their radii, and not more [21].

The statistics of the differences of the CNES land uplift rate with the GPS data are shown as an appended data in the abscissa of Fig. 1, which show an RMS of 1.1 and 3.4 mm/a for Fennoscandia and Laurentia, respectively. The RMS differences of the CNES data are larger than that of the CSR and GFZ data, when the DDK2-4, for Fennoscandia and DDK2-5, and GF of radii 350-700, for Laurentia are used.

The data from a geophysical GIA model: The response of the Earth to a load, tide, or a rotational torque [39] is a kernel function that can be written in terms of the Love numbers [25]. The system of

Preprints (www.preprints.org) | NOT PEER-REVIEWED | Posted: 25 January 2019 doi:10.20944/preprints201901.0261.v1

differential equations of motion and the Poisson equation can be solved either using Laplace transform or in the time domain. The program SELEN from [40] solves the equations in the Laplace domain [41].

We use above-mentioned program to obtain the land uplift rate and geoid changes, which are among their other outputs, of interest to this study. Using the GIA forward models, we need to fix the input parameters in one way or another. A two-layered viscosity seems to be enough in GIA studies, as it was already mentioned and tested in various studies [42], especially when only the vertical component is needed. It should be mentioned that the two-layered viscosity models that could be applicable to the entire region differ significantly from each other (see e.g. the discussion in [17]). However, a groups of different models which can show insignificant differences with a test data set was found [17]. Since the input parameters of GIA forward model are already tuned such that their outputs fit the geodetic data sets, mainly from GPS, the controversy in the rheology of the mantle, among these authors, cannot affect the objectives of this study.

To determine the GIA forward model, we use the input parameters for the lithosphere effective thickness and a three-layered viscosity as in VM5a model [18]. VM5a is our preferred viscosity model because the predicted land uplift rates using VM5a were shown to be the closest to the GPS and relative sea-level data amongst other viscosity parameters [17-18]. Then,

1) We compute the load Love numbers using the program SELEN-2.9.12 [40], where we use a Heaviside loading of a disc shape (Heaviside loading, [42], Sect 2.2) and replace the degree $n = 1$ as in [43].
2) We download the ice models, since $t_{LGM} = 21$ Ka BP and with 500 years intervals, from this webpage: http://www.atmosp.physics.utoronto.ca/~peltier/data.php.
3) We compute the Green's function and the load Love numbers from step 1).
4) The time difference of the disturbing potential divided by the normal gravity is the temporal geoid change. The disturbing potential at each pixel, i and epoch t is obtained by a numerical integration, such as

$$T_i(t) = \sum_{t_k = t_{LGM}}^{t} \sum_{j=1}^{N} G^T(t - t_k, \psi) L_j(t_k) \Delta_j \qquad (1)$$

where G^T is the spatiotemporal Green's kernel of the disturbing potential superscripted by T, Δ_j is the area of each $1^o \times 1^o$ pixel j, $L_j(t_k)$ is the load function at the centre of each pixel j at the discretized time t_k that we used in step 2), and ψ is the spherical distance between the centre of the pixel j to that of the pixel i.

The temporal geoid change is determined using SHT. Then, it is converted to the land uplift rate using Eq. (3).

3.3. The gravimetric land uplift rates

Using the extracting methods (see Appendix), we produce the gravimetric land uplift rate models from the GRACE monthly gravity data. These models are plotted in Figs. 3 and 4, for the areas under study (see the supplementary material for the geoid rates and Table S1 for the model's statistics).

The fastest land uplift rate in North America is obtained using PCA/EOF and CNES data at 15.4 mm/a. The same maximum land uplift rate is also estimated for GFZ data either using ICA or PCA/EOF method. The maximum estimated land uplift rate using CSR data is about 1 mm/a smaller. All models in Fig. 3 show two zones of the fast uplift rate, namely in the west and southeast coast of Hudson Bay. The zero line crosses the Great Lakes and continues to North Dakota, where the southern areas undergo large subsidence. This subsidence estimated using ICA and CSR data at -5.2 mm/a in New Mexico as being maximal. Using the CNES data and RA, the secular trend of the land uplift rate shows a noisy pattern over the area, and some stripe artefacts appears when the

Preprints (www.preprints.org) | NOT PEER-REVIEWED | Posted: 25 January 2019 doi:10.20944/preprints201901.0261.v1

PCA/EOF were used (Fig. 3h). The geoid rates (see Figure S1), over the centre of the rebound area, using GFZ data show generally, the largest estimates among the three data sets.

In Fennoscandia, the secular trend from GFZ data is overestimated, and the land uplift rate models (Fig. 4d-f) show about +2.0 mm/a in the northern continental areas. There, the CNES data oscillates between 1.5 to 4.3 mm/a, and, as North America, the PCA/EOF method is the noisy one. The fastest land uplift rate occurs in the eastern coast of Sweden, and the pattern of the land uplift rate is more localized using the ICA method around a point in the Bothnian Gulf (near Ratan) in Fig. 4a, d, and g.

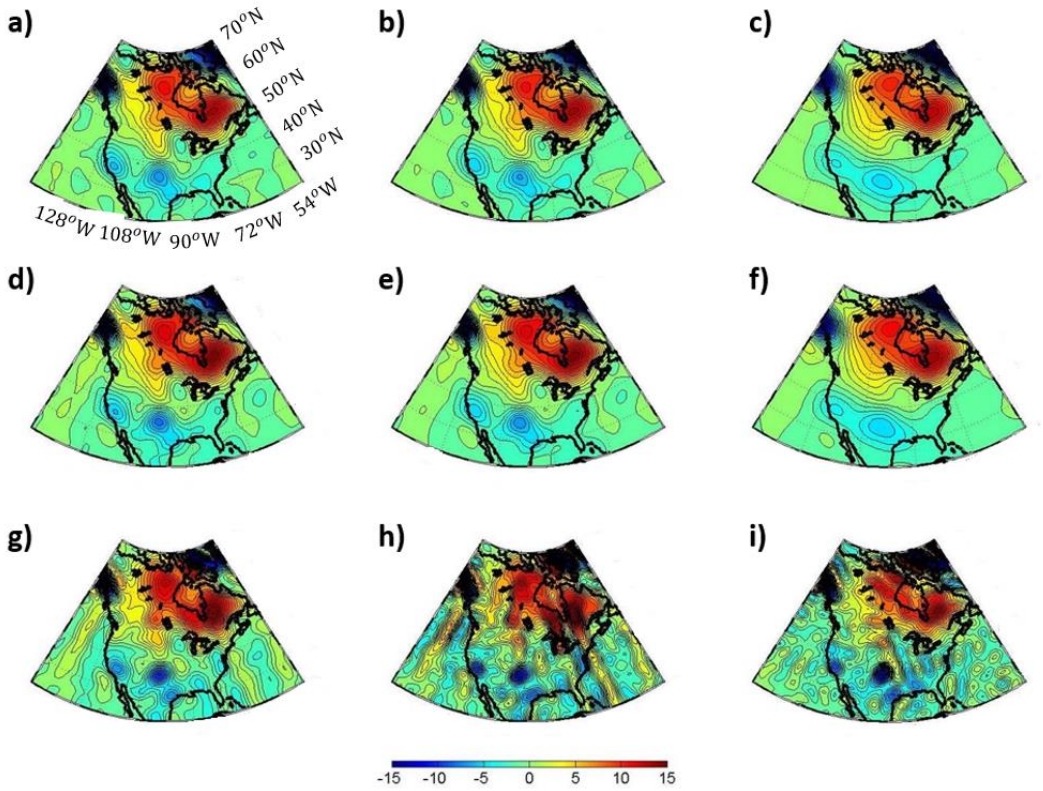

Figure 3. The gravimetric land uplift rate models using CSR (top), GFZ (middle), and CNES (bottom) data and three extracting methods, ICA (a,d,g), PCA/EOF (b,e,h), and RA (c,f,i), for North America. Units: mm/a . ICA: Independent Component Analysis, PCA/EOF: Principal Component Analysis/Empirical Orthogonal Functions, RA: Regression Analysis

Preprints (www.preprints.org) | NOT PEER-REVIEWED | Posted: 25 January 2019 doi:10.20944/preprints201901.0261.v1

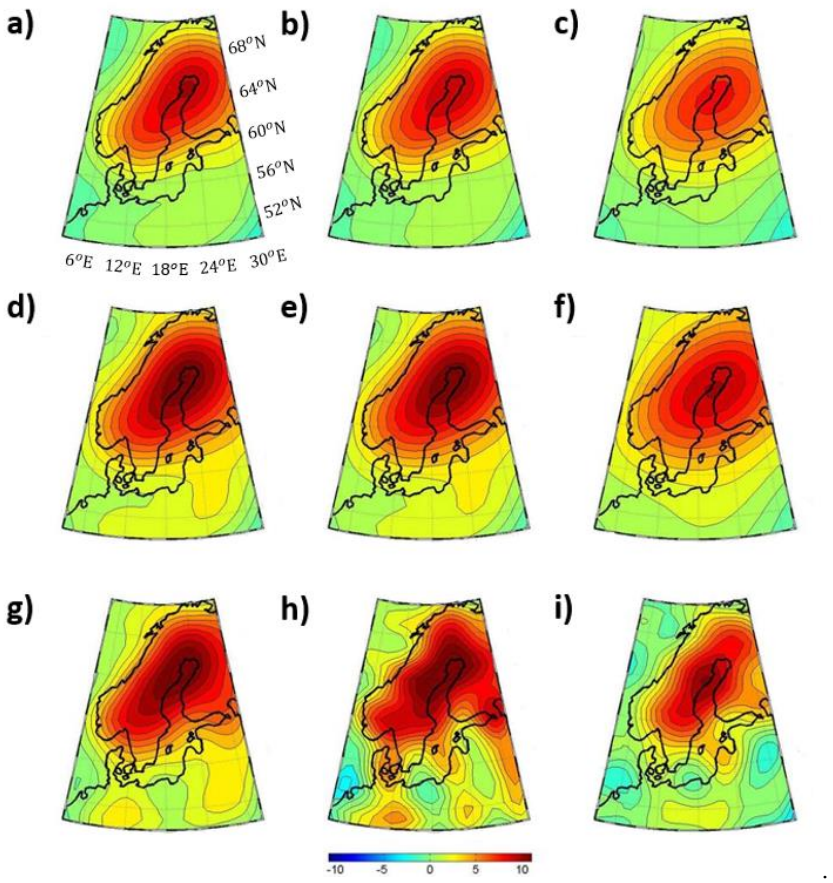

Figure 4. The gravimetric land uplift rate models using CSR (top), GFZ (middle), and CNES (bottom) data and three extracting methods, ICA (a,d,g), PCA/EOF (b,e,h), and RA (c,f,i), fop Fennoscandia. Units: mm/a . ICA: Independent Component Analysis, PCA/EOF: Principal Component Analysis/Empirical Orthogonal Functions, RA: Regression Analysis

3.4. Comparing the Land Uplift Rates from the Gravimetric Model with the GPS Data and the Geophysical GIA Model

3.4.1. Comparing with the GPS data

The differences between the gravimetric models, depicted in Figs. 3 and 4, and the GPS data are given in Table 1. The determined GIA signal of the ELU rates compared with that from the GPS data at the GPS stations. The RMS difference values and the results of the statistical test are given at the GPS stations. However, to show the differences over the study areas and the effect of the possibly remaining stripes after the filtering (see Sect. 3.2), we interpolate the GPS data on $1^o \times 1^o$ grids leading to a pure geometric model of the solid Earth's vertical movement due to GIA for each study area. To measure the consistency between the gravimetric and geometric (GPS) models, we use a correlation analysis. The Correlation Coefficient (CC) is a measure of the paternal match of two models over the whole area. Note that a large estimated correlation coefficient (r) does not necessarily imply that it is significant, but it needs to be tested. Such a test variable reads [44] (Ch. 4.7.5) $T_r = r\sqrt{(N-2)/(1-r^2)}$, where N is the number of points. If $|T_r| > \tau_{0.05}$, where τ is the theoretical test statistics at 5 % risk level, the correlation coefficient is regarded as significant otherwise not.

The GPS data, especially in North America, are too sparse to analyse the paternal compatibility over the whole area using correlation analysis. To interpolate the GPS data, which are otherwise scattered at the points of the GPS stations, we use a C++ code of a nearest-neighbour interpolation from [45] called delaunay.h and modified the freestanding function *dist()* to compute the weights using the inverse distance and the standard deviation of each point. The GPS data, at each station, are used as a test data to be compared with the GRACE data, being estimated at the location of these

Preprints (www.preprints.org) | NOT PEER-REVIEWED | Posted: 25 January 2019 doi:10.20944/preprints201901.0261.v1

stations. When it is needed to compare the pattern of changes over the area, then the GPA data are interpolated or extrapolated leading to a geometric model. All data are then interpolated using a Delaunay triangulation and nearest-neighbour interpolation method on $1^o \times 1^o$ grids.

To test the significance of the differences, a Student's test is performed with a theoretical value of $t_{0.05} = 1.984$ [46] (Ch. 2–18) at the 5 % risk level. The test variable is $T_i = \left(\dot{h}_i^{GRACE} - \dot{h}_i^{GPS}\right)/s_i$, where $s_i = \sqrt{s^2_{\dot{h}_i^{GRACE}} + s^2_{\dot{h}_i^{GPS}}}$, at the GPS stations (see Figure S5). If $|T_i| > t_{0.05}$ we conclude that there is a significant difference and this station, in other words, is rejected in the test, otherwise we accept the null hypothesis, which means that the difference is not significant with a 95 % confidence. The results are also given in Table 1. If the differences are more than three times of the standard deviation of the differences, they are detected as outliers [47].

For Laurentia the differences are in the range of $0.0 - 1.2$ mm/a for the stations around Hudson Bay and by using decomposition techniques (ICA and/or PCA/EOF), and reach to a maximum of 2 mm/a when using RA. The gravity signal due to the ice mass change, likely, contaminates the estimated ELU rates. This gravity change signal shows a nearly secular trend within the timespan of the GRACE data (e.g. [48]).

In Laurentia, using ICA method, the number of the stations, which are rejected in the test reduces and the correlations increase, except for the CNES data, where it decreases by 0.04, which is very small. The stations around Hudson Bay were determined using GPS data with relatively longer time series and higher reliability, which are all accepted in the Student's t-test with two exceptions: for PCA/EOF and RA extracting method and the CNES data. However, using ICA, the same stations around Hudson Bay are now accepted.

The rejected stations (see Figure S5) show three clustering regions, one along the Great Lakes, one in north-west Canada, including Calgary and Whitehorse stations, and another one in southern US, with less certainty, smaller test variables. The stations in Alaska are rejected. The areas around the Great Lakes are accompanied with the signal of the hydrology cycles, which may alter the determined gravimetric models and not the GPS data. The Western Canada undergoes a complicated subduction pattern (e.g. [5]), which can also disturb the GPS estimations. In Alaska, the gravity signal of the ice sheet mass change, likely, affects the secular trend estimation from the GRACE data.

In Fennoscandia, the differences are $0.0 - 1.2$ mm/a for the north-eastern coast of Sweden, the centre of uplift, and always smaller than 2.2 mm/a. Most of the rejected stations in the Student's test are in the peripheral area. The stations near the uplift centre are mostly accepted in the test. However, using ICA and PCA/EOF technique and in contrast to the RA, some of them are rejected in the north-eastern coastline of Sweden. The results from GFZ data implied an overestimation but almost all the rejected stations are far from the centre of uplift. In addition, the stations with small recording time durations (most of them in Norway) are rejected. These are promising results, regardless of the extracting method.

Table 1: Comparison of the land uplift rates from GRACE and GPS, in Laurentia and Fennoscandia. CC is the Correlation Coefficient.

		ICA			**PCA/EOF**			**RA**		
		GFZ	CSR	CNES	GFZ	CSR	CNES	GFZ	CSR	CNES
Laurentia	RMS (mm/a)	3.01	2.95	4.15	3.2	2.94	4.00	3.04	2.75	4.12
	No. of rejected stations	69	50	45	80	58	47	83	63	50
	No. of outlier stations	8	8	7	8	8	7	7	7	7
	CC	0.74	0.74	0.56	0.78	0.70	0.60	0.66	0.69	0.57
Fennoscandia	RMS (mm/a)	2.19	1.2	1.88	2.00	0.34	2.52	1.93	1.57	3.44
	No. of rejected stations	84	33	12	96	39	9	90	52	7
	No. of outlier stations	3	1	7	1	1	7	1	1	7
	CC	0.96	0.99	0.85	0.89	0.89	0.72	0.85	0.82	0.82

3.4.2. Comparing with the Data from a Geophysical Model

Preprints (www.preprints.org) | NOT PEER-REVIEWED | Posted: 25 January 2019 doi:10.20944/preprints201901.0261.v1

As described in Sect. 3.2, we predict the regional GIA land uplift and geoid rates using a GIA forward modelling approach and compare them with the determined ELU rates from the GRACE data at the location of the GPS stations. Then we repeat the statistic Student's test for each point to find out where the differences are significant within a 5 % risk interval. The correlation test is performed on the $1^o \times 1^o$ gridded data to measure the paternal match between two data sets.

The results of this comparison are given in Table 2 (as well as in Figure S9-S13). In North America, along the western, southern, and south-eastern coasts of Hudson Bay, and using CSR and GFZ data, the differences almost vanish. In the western coast of Canada and the US, which undergo complicated tectonics, such as those areas around the Dixon Entrance [28], the differences range between -4.0 and $+1.8$ mm/a, for all the gravimetric land uplift rate models.

The CNES data show noisy pattern of the differences over the area, while the positive and negative maxima occur at the same location as for the other data sets. These subareas are in Alaska, southeast US, and west of the Lake Winnipeg. Collocated with the same areas, the geoid rates also show large differences which are -1.2, -0.36, and $+0.41$ mm/a, respectively.

In Fennoscandia, using RA, and CSR data, a -1.5 mm/a difference occurs in the centre of uplift, while the difference is almost zero using ICA and PCA/EOF methods. The differences are 1.5 mm/a at maximum for GFZ data using either ICA or PCA/EOF methods in Bothnian Gulf, collocated with the zero-difference area using CSR data.

In the western coasts of Norway, and Denmark, the maxima of the gravimetric model are overestimated with respect to the GIA forward model. The correlations increase when changing from RA to PCA/EOF and from that to ICA by a mean value of 0.11, and they decrease with respect to the correlations with the GPS data by a mean value of 0.10, implying that our models are in better general agreement with the GPS data than with the GIA forward model.

Table 2: Comparison of the Gravimetric land uplift rate from GRACE and that of the GIA forward model, in Laurentia and Fennoscandia. CC is the Correlation Coefficient.

		ICA			**PCA/EOF**			**RA**		
		GFZ	CSR	CNES	GFZ	CSR	CNES	GFZ	CSR	CNES
Laurentia	RMS (mm/a)	0.76	1.13	1.55	0.80	1.15	1.68	0.81	1.15	1.66
	No. of rejected stations	6	8	7	6	6	7	6	7	7
	No. of outlier stations	4	4	4	4	4	4	4	3	4
	CC	0.80	0.75	0.66	0.89	0.89	0.72	0.78	0.68	0.57
Fennoscandia	RMS (mm/a)	3.12	2.40	3.00	3.20	2.50	3.58	3.60	2.70	4.56
	No. of rejected stations	118	40	112	106	40	115	63	20	33
	No. of outlier stations	1	1	1	1	1	1	1	1	1
	CC	0.85	0.90	0.79	0.78	0.85	0.60	0.66	0.70	0.57

3.4.3. The Best Gravimetric GIA Land Uplift Rate Model

From the comparisons that were carried out in the previous sections, the extracted secular trend using ICA method and CSR data shows the highest correlation everywhere, except compared to the GIA forward model in Laurentia, where the PCA/EOF method slightly prevails. However, in this case, the RMS values, when the rejected stations were not yet excluded, were less when using ICA than PCA/EOF method (Table 2). Concluding, the ICA method was more successful in extracting the GIA component from the GRACE monthly gravity data. Moreover, the extracting methods were not successful to retrieve the GIA signal in the areas that experience ice mass changes, such as in Alaska. The preferred gravimetric models are plotted in Fig. 5.

Preprints (www.preprints.org) | NOT PEER-REVIEWED | Posted: 25 January 2019 doi:10.20944/preprints201901.0261.v1

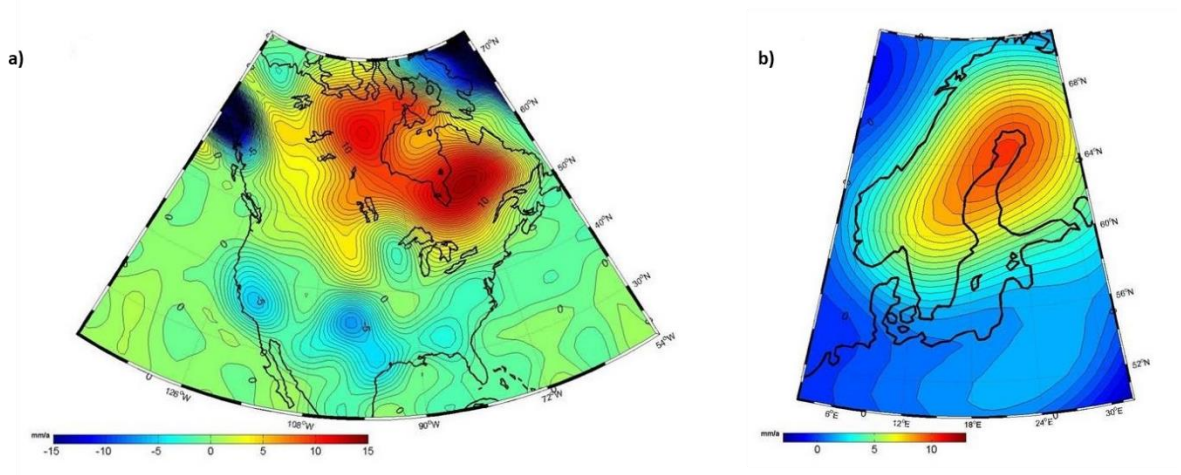

Figure 5. The gravimetric GIA land uplift rate models using ICA extracting method and the CSR data for a) North America and b) Fennoscandia. Units: mm/a.

4. Conclusions

The gravimetric model of the post-glacial land uplift rates is determined more robustly than the same data set from GIA forward modelling approaches, because our methodology is free from the uncertainties in assuming the rheology of the mantle and the glaciation history. It provides an alternative geodetic data set to study the rheology of mantle and the ice load history of Earth, along with other data sets such as the GPS data. We showed that using ICA method, the gravimetric model still needs to be reduced for the hydrology and recent ice mass changes in certain areas. This should not be taken as a drawback, since other data sets also need appropriate corrections. The GPS data need to be reduced, mainly, for the tectonics, while the gravimetric model can provide a nearly homogeneous global coverage, showed to be non-sensitive to the tectonics in Western United States, and it also outputs the gravity quantities e.g. the gravity anomaly signal.

Our conclusions are summarized as follows:

1) We described the theoretical treatment of how the land uplift rate relates the vertical geoid rate due to GIA based on a simple mantle flow and a regional isostatic model and without any assumptions of the glaciation history and the mantle rheology (cf. [13,25,44]). The land uplift rate model determined based on our theoretical relation is shown to be in a good agreement with the GPS data and the data from the GIA forward model for the areas near the uplift centres.
2) We used an ensemble of smoothing filters to investigate their effects in recovering the secular linear trend of the time series of monthly gravity field and found that the anisotropic filters of [37], with the smoothing powers of $0.5 \times 10^{11} \sim 1.0 \times 10^{14}$ (DDK4~DDK1) showed the best agreement with the GPS data for both Laurentian and Fennoscandian regions of study and provides a spatial resolution of ~211 km (in accord with the highest harmonic degrees of the GRACE data). The regional RMS differences with the GPS data are of 2.5 and 1.2 mm/a within a 95% confidence level, respectively.
3) Among three analysis methods, namely ICA, PCA/EOF, and RA, that we used to extract the secular trend of gravity signal from the GRACE data, the ICA method yielded the highest correlation coefficients and smallest weighted RMS differences, compared with GPS data and with the data from our preferred GIA forward model in Fennoscandia. In North America, the PCA/EOF method showed slightly closer fit to the data from the GIA forward model. For the subareas that undergo strong hydrological processes or ice mass variations, such as in the areas near Lake Winnipeg, the differences are relatively large. On the contrary, the ICA method was successful in extracting the GIA signal in the sub-areas with strong tectonics, such as in Western Canada and in California.

4) The main finding of this study is that the preferred regional post-glacial gravimetric land uplift rate models can be determined using the GRACE monthly gravity data from the University of Texas at Austin, Center for Space Research smoothed by DDK4 anisotropic filter and extracted using the ICA method. These models show a maximum standard error of 2.5 mm/a for North America and 0.7 mm/a for Fennoscandia.

References

1. Peltier, W. R., Farrell, W. E., & Clark, J. A. Glacial isostasy and relative sea level: a global finite element model. Tectonophysics, 1978, 50(2-3), 81-110.
2. Ekman, M., Mäkinen, J., Midtsundstad, A., & Remmer, O. Gravity change and land uplift in Fennoscandia 1966–1984. Bulletin géodésique, 1987, 61(1), 60-64.
3. Sjöberg, L. E. A Refined Adjustment Model for the Secular Change of Gravity on the Fennoscandian 63° Latitude Gravity Line. In Global and Regional Geodynamics 1990, pp. 337-348. Springer, New York, NY.
4. Ekman, M., & Mäkinen, J. Recent postglacial rebound, gravity change and mantle flow in Fennoscandia. Geophysical Journal International, 1996, 126(1), 229-234.
5. Pagiatakis, S. D., & Salib, P. Historical relative gravity observations and the time rate of change of gravity due to postglacial rebound and other tectonic movements in Canada. Journal of Geophysical Research: Solid Earth, 2003, 108(B9).
6. Lambert, A., Courtier, N., Sasagawa, G. S., Klopping, F., Winester, D., James, T. S., & Liard, J. O. New constraints on Laurentide postglacial rebound from absolute gravity measurements. Geophysical Research Letters, 2001, 28(10), 2109-2112.
7. Lambert, A., Courtier, N., & James, T. S. Long-term monitoring by absolute gravimetry: Tides to postglacial rebound. Journal of Geodynamics, 2006, 41(1-3), 307-317.
8. Wahr, J., & Velicogna, I. What might GRACE contribute to studies of post glacial rebound? Space Science Reviews, 2003, 108(1-2), 319-330.
9. Rangelova, E., & Sideris, M. G. Contributions of terrestrial and GRACE data to the study of the secular geoid changes in North America. Journal of Geodynamics, 2008, 46(3-5), 131-143.
10. Swenson, S., & Wahr, J. Post-processing removal of correlated errors in GRACE data. Geophysical Research Letters, 2006, 33(8).
11. Hill, E. M., Davis, J. L., Tamisiea, M. E., & Lidberg, M. Combination of geodetic observations and models for glacial isostatic adjustment fields in Fennoscandia. Journal of Geophysical Research: Solid Earth, 2010, 115(B7).
12. van der Wal, W., Kurtenbach, E., Kusche, J., & Vermeersen, B. Radial and tangential gravity rates from GRACE in areas of glacial isostatic adjustment. *Geophysical Journal International*, 2011, *187*(2), 797-812.
13. Wahr, J., Wingham, D., & Bentley, C. A method of combining ICESat and GRACE satellite data to constrain Antarctic mass balance. Journal of Geophysical Research: Solid Earth 2000, 105(B7) pp.16279-16294.
14. Müller, J., Naeimi, M., Gitlein, O., Timmen, L., & Denker, H. A land uplift model in Fennoscandia combining GRACE and absolute gravimetry data. Physics and Chemistry of the Earth, Parts A/B/C, 2012, 53, 54-60.
15. Steffen, H., Denker, H., & Müller, J. Glacial isostatic adjustment in Fennoscandia from GRACE data and comparison with geodynamical models. Journal of Geodynamics, 2008, 46(3-5), 155-164.
16. Boergens, E., Rangelova, E., Sideris, M. G., & Kusche, J. Assessment of the capabilities of the temporal and spatiotemporal ICA method for geophysical signal separation in GRACE data. Journal of Geophysical Research: Solid Earth, 2014, 119(5), 4429-4447.
17. Peltier, W. R., Argus, D. F., & Drummond, R. Space geodesy constrains ice age terminal deglaciation: The global ICE-6G_C (VM5a) model. Journal of Geophysical Research: Solid Earth, 2015, 120(1), 450-487.
18. Peltier, W. R., & Drummond, R. Rheological stratification of the lithosphere: A direct inference based upon the geodetically observed pattern of the glacial isostatic adjustment of the North American continent. Geophysical Research Letters, 2008, 35(16).
19. Guo, J. Y., Huang, Z. W., Shum, C. K., and Van der Wal, W. Comparisons among contemporary glacial isostatic adjustment models. Journal of Geodynamics, 2012, 61 pp.129-137.
20. Wang, H., Jia, L., Steffen, H., Wu, P., Jiang, L., Hsu, H., Longwei, X., Zhiyong, W., Hu, B. Increased water storage in North America and Scandinavia from GRACE gravity data. *Nature Geoscience* 2013, *6*(1), 38.

21. Shafiei Joud, M. S., Sjöberg, L. E., & Bagherbandi, M. Use of GRACE data to detect the present land uplift rate in Fennoscandia. Geophysical Journal International, 2017, 209(2), 909-922.
22. Bettadpur, S. Gravity Recovery and Climate Experiment UTCSR level-2 processing standards document. University of Texas at Austin, GRACE Doc, 327742, 16. 2012.
23. Dahle, C. Flechtner, F. Gruber, C. König, D. König, R. Michalak, G., Neumayer, K. H. GFZ GRACE Level-2 Processing Standards Document for Level-2 Product Release 0005, (Scientific Technical Report - Data , 12/02), Potsdam, 20 p. DOI: 10.2312/GFZ.b103-12020, 2012.
24. Wiese, D.N., Folkner, W.M. & Nerem, R.S. Alternative mission architectures for a gravity recovery satellite mission. Journal of Geodesy 2009, 83: 569. https://doi.org/10.1007/s00190-008-0274-1
25. Longman, I. M. A Green's function for determining the deformation of the Earth under surface mass loads: 2. Computations and numerical results. Journal of Geophysical Research, 1963, 68(2), 485-496.
26. Burgess, P. M., Gurnis, M., Moresi, L. Formation of sequences in the cratonic interior of North America by interaction between mantle, eustatic, and stratigraphic processes. *Geological Society of America Bulletin*, 1997, *109*(12), 1515-1535.
27. Shafiei Joud, M. S. Contributions of Satellite Geodesy to Post-Glacial Rebound Research. **Doctoral Dissertation** in Geodesy. Royal Institute of Technology, TRITA-SOM, ISSN 1653-6126 ; 2018-02, 180 p.
28. Argus, D. F., Gordon, R. G., Heflin, M. B., Ma, C., Eanes, R. J., Willis, P., Peltier, W. R., Owen, S. E. The angular velocities of the plates and the velocity of Earth's centre from space geodesy. Geophysical Journal International, 2010, 180(3), 913-960.
29. Kierulf, H. P., Steffen, H., Simpson, M. J. R., Lidberg, M., Wu, P., & Wang, H. A GPS velocity field for Fennoscandia and a consistent comparison to glacial isostatic adjustment models. Journal of geophysical research: solid earth, 2014, 119(8), 6613-6629.
30. Steffen, H., Kaufmann, G., & Wu, P. Three-dimensional finite-element modeling of the glacial isostatic adjustment in Fennoscandia. Earth and Planetary Science Letters, 2006, 250(1-2), 358-375.
31. Sella, G. F., Stein, S., Dixon, T. H., Craymer, M., James, T. S., Mazzotti, S., & Dokka, R. K. Observation of glacial isostatic adjustment in "stable" North America with GPS. Geophysical Research Letters, 2007, 34(2).
32. Ray, J., Dong, D., & Altamimi, Z. IGS reference frames: status and future improvements. GPS solutions, 2004, 8(4), 251-266.
33. Craymer, M. R., Personal Communication, 2017
34. Craymer, M. R., Henton, J. A., Piraszewski, M., & Lapelle, E. An updated GPS velocity field for Canada. In AGU Fall Meeting. 2011.
35. Flechtner, F., Dobslaw, H., & Fagiolini, E. AOD1B Product Description Document for Product Release 05 (Rev. 4.3, April 23, 2015). 2015.
36. Bruinsma, S., Lemoine, J. M., Biancale, R., & Vales, N. CNES/GRGS 10-day gravity field models (release 2) and their evaluation. Advances in Space Research, 2010, 45(4), 587-601.
37. Kusche, J., Schmidt, R., Petrovic, S., & Rietbroek, R. Decorrelated GRACE time-variable gravity solutions by GFZ, and their validation using a hydrological model. Journal of geodesy, 2009, 83(10), 903-913.
38. Jekeli, C. Alternative methods to smooth the Earth's gravity field. 327 Dept. of Geod. Sci. and Surv. Ohio State Univ. Columbus. 1981.
39. Stuhne, G. R., Peltier, W. R. Reconciling the ICE-6G_C reconstruction of glacial chronology with ice sheet dynamics: The cases of Greenland and Antarctica. *Journal of Geophysical Research: Earth Surface*, 2015, 120.9: 1841-1865.
40. Spada, G., & Stocchi, P. SELEN: A Fortran 90 program for solving the "sea-level equation". Computers & Geosciences, 2007, 33(4), 538-562.
41. Spada, G., Barletta, V. R., Klemann, V., Riva, R. E. M., Martinec, Z., Gasperini, P., Lund, B., Wolf, D., Vermeersen, L. L. A., King, M. A. A benchmark study for glacial isostatic adjustment codes. Geophysical Journal International, 2011, 185(1), 106-132.
42. Paulson, A., Zhong, S., & Wahr, J. Inference of mantle viscosity from GRACE and relative sea level data. Geophysical Journal International, 2007, 171(2), 497-508.
43. Wahr, J., DaZhong, H., & Trupin, A. Predictions of vertical uplift caused by changing polar ice volumes on a viscoelastic Earth. Geophysical Research Letters, 1995, 22(8), 977-980.
44. Jacoby, W., & Smilde, P. L. Fundamentals of Gravity, Elements of Potential Theory in Gravity interpretation: fundamentals and application of gravity inversion and geological interpretation. Springer-Verlag Berlin Heidelberg. 2009. pp. 23-111, **DOI:** 10.1007/978-3-540-85329-9

45. Press, W. H., Teukolsky, S. A., Vetterling, W. T., & Flannery, B. P. *Numerical recipes 3rd edition: The art of scientific computing*. Cambridge university press. . 2007.
46. Bjerhammar, A. Theory of errors and generalized matrix inverses. 1973. Elsevier New York, 420 p.
47. Thompson, R. A note on restricted maximum likelihood estimation with an alternative outlier model. *Journal of the Royal Statistical Society. Series B (Methodological)*, 1985, 53-55.
48. Ran, J., Ditmar, P., Klees, R., & Farahani, H. H. Statistically optimal estimation of Greenland Ice Sheet mass variations from GRACE monthly solutions using an improved mascon approach. *Journal of Geodesy*, 2018, *92*(3), 299-319.
49. Jolliffe, I. T., Principal Component Analysis, 2nd Ed., Springer-Verlag New York 2002, 488p. ISBN 978-0-387-22440-4, DOI: 10.1007/b98835
50. Forootan, E. Statistical signal decomposition techniques for analyzing time-variable satellite gravimetry data. 2014, 143 p. (Doctoral dissertation Universitäta-und-Landesbibliothek Bonn)
51. Murphy, K. Machine learning: a Probabilistic perspective. The MIT Press Cambridge, Massachusetts London, England. ISBN 978-0-262-01802-9. 2012, 1098 p.
52. Stone, J. V. Independent Component Analysis: A Tutorial Introduction, The MIT Press, Cambridge, Mass. ISBN 0262693151, 9780262693158, 2004, 193 p.
53. Hyvärinen, A., & Oja, E. Independent component analysis: algorithms and applications. Neural networks, 2000, 13(4-5), 411-430.
54. Hyvarinen, A. Fast and robust fixed-point algorithms for independent component analysis. IEEE transactions on Neural Networks, 1999, 10(3), 626-634.
55. Hyvärinen, A. Karhunen, J. and Oja, E. Independent component analysis (Vol. 46). John Wiley and Sons. ISBN: 978-0-471-40540-5, 2001. 504 p.
56. Forootan, E., & Kusche, J. Separation of global time-variable gravity signals into maximally independent components. Journal of Geodesy, 2012, 86(7), 477-497.
57. Cardoso, J. F. High-order contrasts for independent component analysis. Neural computation, 1999, 11(1), 157-192.
58. Reza, F. M. An introduction to information theory. Courier Corporation. New York, McGraw-Hill, 1961. 496 p.
59. Girolami, M. Advances in Independent Component Analysis. Springer-Verlag London Limited. **DOI** https://doi.org/10.1007/978-1-4471-0443-8. **ISBN** 978-1-85233-263-1, 2000, 286 p.

Appendix:

Extracting methods

We investigate the application of three analysis methods in extracting the GIA signal out of the GRACE temporal gravity field. The secular linear trend will be extracted against the periodicities with known temporal periods of occurrence using a RA. The success of a RA depends on our knowledge of these periodicities. Using the statistical decomposition methods such as PCA/EOF and ICA, a few linear combinations, and not necessarily a secular trend, of the spatiotemporal signal are extracted. The extracted linear combinations satisfy some statistical criteria. In PCA/EOF, the principal components (PCs) have the same variance as the input GRACE spatiotemporal signal. In ICA, the independent components (ICs) are selected such that the measure of mutual independency is maximized.

Principal Component /Empirical Orthogonal Function Analysis (PCA/EOF): PCA/EOF is a data reduction technique, which retains as much as possible of the variation present in the data vector of interrelated variables. This is achieved by transforming the multivariate vector of data to a new set of variables, the principal components (PCs), which are uncorrelated [49]. In PCA/EOF, the variance of each component, after the decomposition, will be the Eigen Values (EVs) of the covariance matrix of the data. It means that each matrix $\mathbf{L}_{E,N}$, with E rows (like the number of epochs) and N columns (like the number of points), can be written as

$$\mathbf{L}_{E,N} = \mathbf{U}\mathbf{\Lambda}\mathbf{V}^T , \qquad (A.2)$$

Preprints (www.preprints.org) | NOT PEER-REVIEWED | Posted: 25 January 2019 doi:10.20944/preprints201901.0261.v1

where $\mathbf{\Lambda}$ is the diagonal $N\times N$ matrix of singular values (SVs), $\mathbf{U}$ and $\mathbf{V}$ are $E\times N$ and $N\times N$ orthogonal matrices (for example invariant of time). Each row of the multivariate observation vector $\mathbf{L}$ is the spatial data at each time and each column, a time series of each point. To clarify we have $\mathbf{L}_{EN}=\left[\mathbf{l}_1 \quad \mathbf{l}_2 \quad \cdots \quad \mathbf{l}_N\right]$ and each univariate vector $\mathbf{l}_i=\left[l_i^1 \quad l_i^2 \quad \cdots \quad l_i^E\right]^T$, $i=1,...,N$ is a time series of GRACE monthly gravity field for each point. The PCs are the rows of

$$\mathbf{P}=\mathbf{U}\mathbf{\Lambda}. \tag{A.2}$$

Let the columns of $\mathbf{V}$ be the Eigen vectors of the $N\times N$ covariance matrix $\mathbf{C}$ i.e., $\mathbf{C}\mathbf{V}=\mathbf{V}\mathbf{\Lambda}^2$. The diagonal elements of $\mathbf{C}$ are the variances of vectors (columns) of $\mathbf{L}$. The Eigen Value Decomposition (EVD) of the covariance matrix is the only condition of the PCA/EOF method, which guarantees that the orthogonal projection of the data $\mathbf{L}$ on the orthogonal basis (columns of $\mathbf{V}$) has the maximum variability. Note that an orthogonal $\mathbf{V}$ such as $\mathbf{V}^T\mathbf{V}=\mathbf{I}_N$ makes the orthogonal vectors invariant with respect to the row space (time) of the data. It can be shown that principal components have the same sum of the variances as the data variance-covariance matrix.

Several variants of the PCA/EOF decomposition method can be found in [50] in more details but the core and the main concept is as already presented above. The reconstruction of the data is carried out using a finite set of the SVs as in Eq. (A.2). Only the large SVs are used for reconstruction, under the assumption that the singular values close to zero only represent noise. The former is arranged in $\mathbf{\Lambda}$ and the latter in the rows of $\mathbf{U}$. We have

$$\mathbf{P}=\mathbf{U}\mathbf{U}^T\left(\mathbf{U}\mathbf{U}^T\right)^{-1}\tilde{\mathbf{P}}, \tag{A.3}$$

where $\tilde{\mathbf{P}}=\mathbf{U}\mathbf{\Lambda}$, $\mathbf{\Lambda}$ is now a $P\times P$ diagonal matrix, $P\le\min(E,N)$ is the number of the preferred set of the SVs, and now, the dimensions of $\tilde{\mathbf{P}}$ and $\mathbf{V}$ reduce to $E\times P$ and $N\times P$, respectively. The factor of $\tilde{\mathbf{P}}$ on the RHS of Eq. (A.3) is the idempotent operator, which is defined, such as [46] (Ch.9) $\mathbf{U}^o=\mathbf{U}\mathbf{U}_{IO}^-$, where $\mathbf{U}_{IO}^-=\mathbf{U}^T\left(\mathbf{U}\mathbf{U}^T\right)^{-1}$ is the normal general inverse [46] (p. 106). Eq. (A.3) is the reconstruction property.

The PCA/EOF method, when the noises in the model are assumed has been formulated slightly differently from the model described in Eq. (A.2). The covariance matrix of the estimation of the PCs are then estimated using a factor analysis method and usually been referred to as Probabilistic PCA (PPCA, see [51]). The covariance matrix is weighted by the sum of the variances of those PCs that were not used in the final solution and have been neglected [51] (Ch. 12).

Independent Component Analysis (ICA): The main goal of ICA of a data signal is that its components after decomposition are mutually independent. Being independent, means that the joint probability distribution function (PDF) of two vectors of random variables is equal to the multiplication of the PDF of each of them. Then, one can easily obtain.

$$E\left\{g(\mathbf{s}_1)g(\mathbf{s}_2)\right\}=E\left\{g(\mathbf{s}_1)\right\}E\left\{g(\mathbf{s}_2)\right\}, \tag{A.4}$$

where $E\{\square\}$ is the mathematical expectation operator and g is an arbitrary function. In PCA/EOF, the PCs are uncorrelated because using the orthogonality condition we have: $\mathbf{P}^T\mathbf{P}=\mathbf{\Lambda}\mathbf{U}^T\mathbf{U}\mathbf{\Lambda}=\mathbf{\Lambda}^2$. Being uncorrelated, means that every two vectors $\mathbf{s}_1$ and $\mathbf{s}_2$ have zero covariance with each other: $E\{\mathbf{s}_1\mathbf{s}_2\}=E\{\mathbf{s}_1\}E\{\mathbf{s}_2\}$. By conditioning the PCs to be uncorrelated, we cannot guarantee that the condition of independency as in Eq. (A.4) holds for other choices of g, for example for $g(\mathbf{s}_i)=\mathbf{s}_i^2$.

Practically, the decomposed components after performing ICA may, usually, be dependent to some extent. If a metric can be defined to measure the "independency", then the goal of ICA is adapted to find the linear combination of the rows of the data matrix, which increases the metric of independency.

The data signal $\mathbf{L}$, consisting of random signals $\mathbf{l}_1,\mathbf{l}_2,...,\mathbf{l}_M$, can be written

$$\mathbf{L}_{E,M}=\mathbf{A}_{E,E}\mathbf{S}_{E,M}. \tag{A.5}$$

Preprints (www.preprints.org) | NOT PEER-REVIEWED | Posted: 25 January 2019 doi:10.20944/preprints201901.0261.v1

We aim at estimating the source signals in $\mathbf{S}$, by determining a general inverse $\mathbf{W}$ of the mixing matrix $\mathbf{A}$, such as

$$\tilde{\mathbf{S}}_{E,M} = \mathbf{W}_{E,E}\mathbf{L}_{E,M}\,. \tag{A.6}$$

The dimensions of Eqs. (A.5) and (A.6) are denoted by the subscripts. The elements of $\tilde{\mathbf{S}}$ are the independent components (ICs). The problem of ICA is to find an optimal matrix inverse $\mathbf{W}$, such that the ICs are independent of each other and/or have a non-Gaussian joint distribution [52] (Ch. 6.3), [53] (Ch. 3.3). Note that being non-Gaussian and independent are identical. The linear combinations in Eq. (A.6) can be independent of each other if and only if their joint PDF has a shape with a maximum deviation from a Gaussian one.

There are several algorithms performing ICA method [53-54], [55] (Chs. 8, 9, and 14), [56-57]. The algorithm which we use for our numerical results, in Sect. 3, are already described in detail in [55] (Chs. 8, 9, and 14) .

To measure the non-Gaussianity, usually the kurtosis,

$$K\{\tilde{\mathbf{s}}_i\} = E\{\tilde{\mathbf{s}}_i^{\,4}\} - 3E^2\{\tilde{\mathbf{s}}_i^{\,2}\}, \tag{A.7}$$

is used, which is the 4th moment of the random vector minus three times of its variance. It is shown (see e.g. [56]) that the kurtosis of a linear combination of independent random vectors ($\mathbf{z}^T{}_i\mathbf{s}_i$) is

$$K\{\mathbf{z}^T{}_i\mathbf{s}_i\} = \sum\nolimits_i z_i^{\,4} K\{s_i\} \tag{A.8}$$

Eq. (A.8) provides the major computational advantage for the family of algorithms, which are based on the kurtosis criterion for the multivariate case, where the kurtosis can be defined using the 4th and the second moments of the multivariate random variable [52] (Ch. 6.6), [57].

Before applying ICA each vector in matrix $\mathbf{L}$ is a random signal with zero mean. This condition can easily be held by removing the mean value of the signal from each element but reduces the degree-of-freedom. The ICA still holds, and the mean value should be added back after the components have been determined. In addition, $\mathbf{L}$ should be linearly transformed into a random spatiotemporal vector $\tilde{\mathbf{L}}$, whose covariance matrix equals the identity (Whitening). This can be carried out using Eigen Value Decomposition (EVD). Then the transformed vector (each column of the matrix $\tilde{\mathbf{L}}$) is: $\tilde{\mathbf{l}} = \mathbf{V}\boldsymbol{\Lambda}\mathbf{V}^T\mathbf{l}$, where the EVD holds for the data signal, i.e. $E\{\mathbf{l}\mathbf{l}^T\} = \mathbf{V}\boldsymbol{\Lambda}^2\mathbf{V}^T$, and with the orthogonality condition, we have: $E\{\tilde{\mathbf{l}}\tilde{\mathbf{l}}^T\} = \mathbf{I}$. The ICA still holds, but with a different mixing matrix, which is, using Eq. (A.5): $\tilde{\mathbf{A}} = \mathbf{V}\boldsymbol{\Lambda}\mathbf{V}^T\mathbf{A}$. We assume that the data signal is already centred and whitened, in the basic equation of ICA, so in Eq. (A.5), we dropped the tildes.

The kurtosis in Eq. (A.7) can be further simplified if we assume that the estimated components have been normalized, such that the variance of each component vector is one. Then, the RHS of Eq. (A.7) becomes $E\{\tilde{\mathbf{s}}_i^{\,4}\} - 3$. This shows that the kurtosis is simply a normalized version of the 4th (zero) moment. If $\tilde{\mathbf{s}}_i$ has Gaussian PDF, then the $E\{\tilde{\mathbf{s}}_i^{\,4}\} = 3E^2\{\tilde{\mathbf{s}}_i^{\,2}\} = 3$, and the kurtosis is zero, otherwise, a negative kurtosis implies that the PDF of the random variable has a rather spiky shape (leptokurtic, super-Gaussian), and a positive kurtosis implies a platykurtic and a sub-Gaussian PDF (see [55] Ch. 8.2, for some examples).

Now, using the metric as in Eq. (A.7), one can solve the Eq. (A.6), for the weight matrix. In practise, one can start from an initial $\mathbf{w}$ being each row of the generalized inverse in Eq. (A.6) and find the direction in which the absolute value of the kurtosis grows maximally. Each single IC can be written as a linear combination of the data vector, such as

$$\tilde{\mathbf{s}}_{1,1} = \mathbf{w}_{1,E}\mathbf{l}_{E,1} \tag{A.8}$$

The gradient of the kurtosis is given by [52-57]

Preprints (www.preprints.org) | NOT PEER-REVIEWED | Posted: 25 January 2019 doi:10.20944/preprints201901.0261.v1

$$\frac{\partial\left|K\left\{\mathbf{wl}\right\}\right|}{\partial\mathbf{w}}=4sign\left(K\left\{\mathbf{wl}\right\}\right)\left(E\left\{\mathbf{l}\left(\mathbf{wl}\right)^{3}\right\}-3\mathbf{w}^{T}E\left\{\left(\mathbf{wl}\right)^{2}\right\}\right) \tag{A.9}$$

Since the data is whitened, it holds that $E\left\{\left(\mathbf{wl}\right)^{2}\right\}=\mathbf{ww}^{T}=\left\|\mathbf{w}^{T}\right\|^{2}$. Then the last term in the RHS of Eq. (A.10) is simply a change in the norm of the estimated weights.

Furthermore, one can determine the direction of the maximal kurtosis in every step on a unit sphere, by normalizing the estimated weights in $\mathbf{w}$. Since only the direction is interesting, we reform the object function in Eq. (A.10) by omitting the last term in the RHS. This does not change the direction of the maximal change of the kurtosis. Then, one obtains the following gradient algorithm [53,55,57]:

Choose a random weight vector as the initial value:

$$\mathbf{w}^{(n)}=\mathbf{w}^{(n-1)}+sign\left(K\left\{\mathbf{wl}\right\}\right)E\left\{\mathbf{l}\left(\mathbf{wl}\right)^{3}\right\}. \tag{A.10}$$

Normalize $\mathbf{w}^{(n)}$, and repeat until the step distance $\left\|\mathbf{w}^{(n)}-\mathbf{w}^{(n-1)}\right\|\le\varepsilon$,

where ε is a very small positive real number. In practise, the expectation is replaced by their estimates.

It should be mentioned that another class of ICA algorithm are based on the basic principles of information theory [58] (Chs. 1,2,3), i.e. measuring entropy and mutual information. This class of algorithms (not discussed here) aim at minimizing the mutual information, or some metrics of independency based on entropy and the coding length of the estimated signal [55] (Ch. 10). However, finally, the ICs suffice minimal mutual information, maximal non-Gaussian joint PDF, and maximal independency conditions, all at the same time. Usually, to practise ICA, first, a metric to measure the independency is defined, then, a recursive "learning" algorithm runs to find the orthogonal projections in which the metric is extremal, such as projection pursuit, gradient, and fixed-point algorithms [55].

The solution to the ICA problem as formed in Eq. (A.5) in the framework of a semi-parametric approach gives a lot of interesting theoretical and practical results. In real-world problems, the situation is different from the above-mentioned ideal case. We cannot avoid the effect of noise, in many cases. Sometimes we need to provide an estimation of the final solution. In addition, the number of the sources is not known. If there is no noise, one could determine directly the number of sources from the data.

A semi-parametric approach to solve this problem has been proposed by [58] (Ch. 11) who used factor analysis for the pre-processing of data, instead of PCA/EOF. Then the power of the noises also the number of the sources are estimated by factor analysis. After the pre-processing, we use the ICA method as described above to estimate the generalized inverse matrix. The problem is then reformulated as a Gauss-Markov model with additive noise. The covariance matrix of the additive errors is estimated using a Maximum Likelihood Estimation method (see [58], Ch. 11, for more details).

Regression Analysis (RA): The system of equations of the RA reads as follows [46] (Ch.11.9):

$$\mathbf{L}_{E,N}=\mathbf{A}_{E,U}\mathbf{X}_{U,N}+\mathbf{E}_{E,N} \tag{A.11}$$

where $\mathbf{A}$ is the design matrix, $\mathbf{X}$ is the matrix of unknown parameters to be determined and matrix $\mathbf{E}$ is the residual that makes the system consistent, and their dimensions are denoted by the subscripts.

In the basic equations Eq. (A.1) and Eq. (A.5) of the PCA/EOF and ICA methods of decomposition, respectively, both matrices in the RHSs are principally unknown. We only know some properties of the decomposed signals and weight matrices. In Eq. (A.11) the regression model parameters (matrix $\mathbf{A}$) are known and the contribution of each parameter (variable) of the model is analysed through a solution to $\mathbf{X}$. RA may be argued to be inferior compared to decomposition methods since the errors of and uncertainties in the model parameters need negatively affect the estimation [9]. However, this cannot be generally a problem because the difference between the

Preprints (www.preprints.org) | NOT PEER-REVIEWED | Posted: 25 January 2019 doi:10.20944/preprints201901.0261.v1

regressed surface and the observations is controlled by the residual vector $\mathbf{E}$ in Eq. (A.11). Each row of $\mathbf{A}$ is samples of a model. This is the conceptual difference between regression analysis and the adjustment by parameter methods [46] (p.148).

Among all the finite set of possible solutions $\tilde{\mathbf{X}}$, the one that provides the minimum total RMS differences between $\mathbf{a}_i^T\tilde{\mathbf{x}}_i$ and $\mathbf{l}_i$ is the least squares solution which reads:

$$\hat{\mathbf{X}} = \mathbf{A}_{OI}^{-}\mathbf{L} \tag{A.12}$$

where $\mathbf{A}_{OI}^{-} = \left(\mathbf{A}^T\mathbf{A}\right)^{-1}\mathbf{A}^T$ is the transnormal general inverse [46] (p.106). Note that the observation is a stochastic process with a Gaussian distribution. Then the solution in Eq. (A.13) is a maximum likelihood solution [46] (Ch.2.19). Those elements of $\hat{\mathbf{X}}$ which significantly differ from zero can be used for making a unique set of solution. However, there is no simple rule that can isolate the significant variables from others. The significance of each variable in modelling the observation $\mathbf{L}$ can be tested using statistical tests. The standard errors of the parameter estimates are the squares of the diagonal elements of the least squares estimated covariance matrix of $\hat{\mathbf{X}}$ (see e.g. [46], Ch.2.19).